Microsc. Microanal. 19, 496–500, 2013
doi:10.1017/S1431927612014249

Microscopy AND Microanalysis

Correlative Fractography: Combining Scanning Electron Microscopy and Light Microscopes for Qualitative and Quantitative Analysis of Fracture Surfaces

Luis Rogerio de Oliveira Hein,* José Alberto de Oliveira, and Kamila Amato de Campos

UNESP—Univ Estadual Paulista, DMT—Department of Materials and Technology, LAIMat—Materials Imaging Laboratory, Av. Ariberto Pereira da Cunha, 333, Guaratinguetá, SP, 12.516-410, Brazil

Abstract: Correlative fractography is a new expression proposed here to describe a new method for the association between scanning electron microscopy (SEM) and light microscopy (LM) for the qualitative and quantitative analysis of fracture surfaces. This article presents a new method involving the fusion of one elevation map obtained by extended depth from focus reconstruction from LM with exactly the same area by SEM and associated techniques, as X-ray mapping. The true topographic information is perfectly associated to local fracture mechanisms with this new technique, presented here as an alternative to stereo-pair reconstruction for the investigation of fractured components. The great advantage of this technique resides in the possibility of combining any imaging methods associated with LM and SEM for the same observed field from fracture surface.

Key words: quantitative fractography, light microscopy, scanning electron microscopy, image processing, extended depth from focus reconstruction, correlative microscopy

Introduction

Correlative microscopy is an expression to describe the association of different microscopy techniques for the investigation of the same issue (Vicidomini et al., 2010). It means to combine the virtues of each instrument for a complete characterization of microstructures regarding to a large range of surface properties. In general, one of the microscopy techniques provides qualitative or quantitative information about some property and the other contributes to the morphological interpretation by improving the resolution and/or the contrast for the same sample region (Sartori et al., 2007; Plitzko et al., 2009). For materials analysis, the correlative microscopy commonly involves light microscopy (LM), scanning electron microscopy (SEM), and/or scanning probe microscopy (SPM). These experiments generally explore the differences in lateral resolution from LM to SPM or SEM, changing magnification to illustrate the morphology of some microstructural feature, or combine the LM images to chemical element distribution maps obtained by microanalysis.

The major difficulties for correlative microscopy experiments reside on the perfect matching of observed regions in the different microscopes (Agronskaia et al., 2008; Verkade, 2008). This matching requires the establishment of a common spatial reference system for the involved microscopes and some software tools based on digital image processing.

This work proposes the "correlative fractography" technique, based on the association of the extended depth from focus reconstruction from LM to the imaging modes and microanalysis from SEM. The solution combines the use of the Zeiss "Shuttle & Find" system (Carl Zeiss, Oberkochen, Germany) to establish the common spatial references and some National Institutes of Health (NIH) ImageJ digital image processing tools. It permits the fusing of elevation maps based on LM image stacks to the SEM images for the same region on fracture surface.

Received June 24, 2012; accepted September 19, 2012
**Corresponding author*. E-mail: rhein@feg.unesp.br

Materials and Methods

One compact-tension specimen of 15-5PH steel fractured according to the ASTM E-647-11e1 standard for fatigue crack growth testing was used to demonstrate the new technique for correlative fractography.

This specimen was fixed on the CorrMic A sample holder of the Zeiss Shuttle & Find system for correlative microscopy, mounted on a Zeiss AxioImager Z2m motorized light microscope. The spatial (x, y) reference system was calibrated according to the marks on sample holder, for the total magnification of 1,600×, following the instructions of the Shuttle & Find plugin for the Zeiss AxioVision 4.8. Image stacks were pictured with a 50×/0,55 LD EC Epiplan Neofluar HD DIC objective lens, under bright-field, dark-field, and C-DIC (circular polarized light–differential interference contrast) contrast modes for the same spatial (x, y, z) coordinates on the sample. The "Topography" plugin for Zeiss AxioVision 4.8 was set to obtain the image stacks with a constant Z spacing of 1.00 μm, with a 10 nm resolution.

After this step, the sample holder was mounted on the scanning electron microscope, a Zeiss EVO LS-15 equipped with one Oxford Inca x-act detector (Oxford

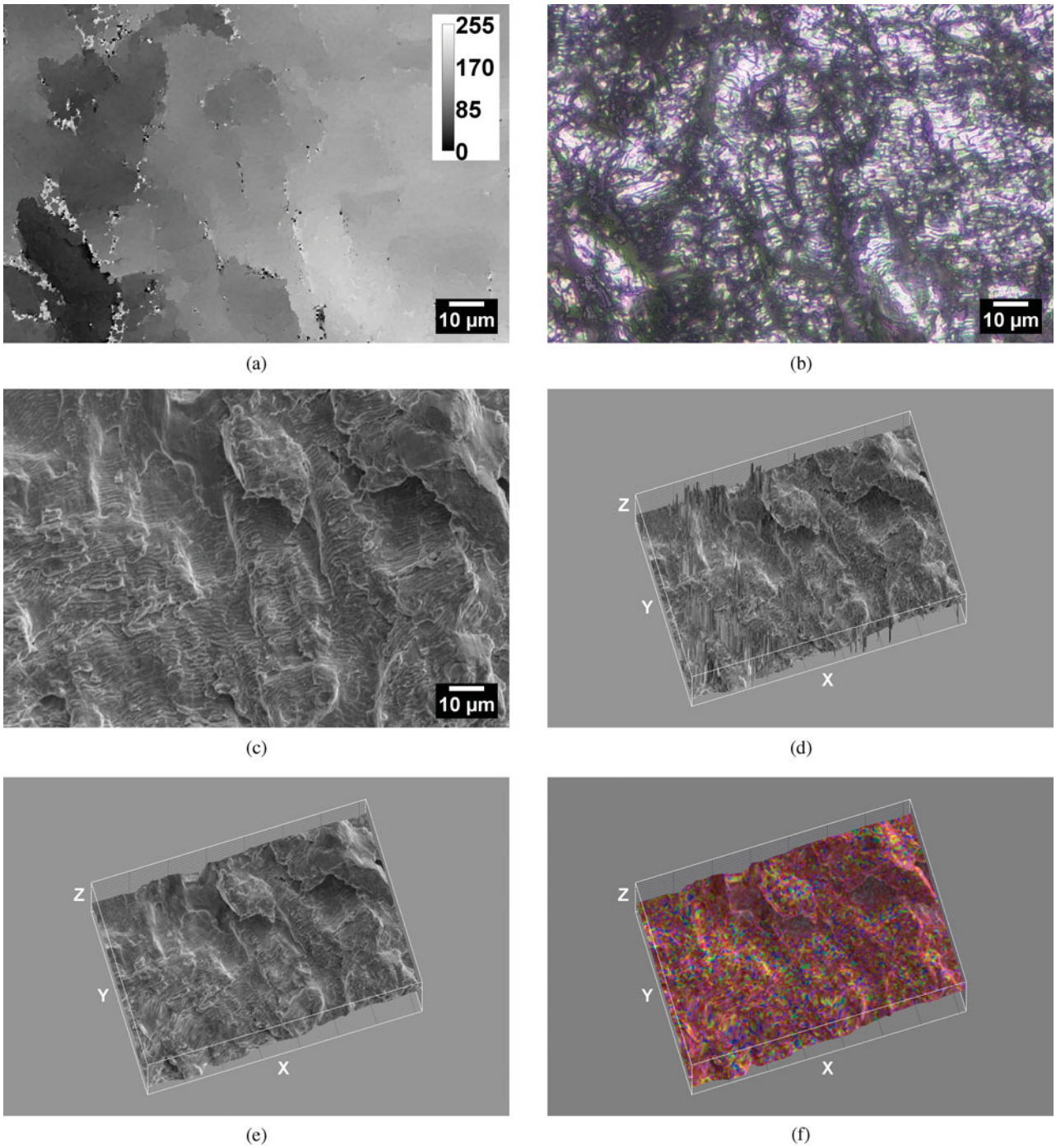

Figure 1. Example of the fields matching in correlative fractography: (**a**) bright-field LM elevation map; (**b**) reconstructed LM image; (**c**) SEM SE image at 14 keV; (**d**) 3D representation of noisy height map merged with the SEM-SE image in panel **d**; (**e**) noise filtered 3D representation of height map with the SEM-SE image as loaded texture, using smoothing slider of Interactive 3D Surface Plot plugin for noise filtering; (**f**) noise filtered 3D representation of height map with the corresponding EDS map as loaded texture: blue, green, and yellow spots are representing, respectively, the distribution of Mn, Cu, and Ni. Fe and Cr are homogeneously distributed. The sizes for X, Y, and Z axis of 3D plots in Figures 1d, 1e, and 1f are, respectively, 143.36, 95.97, and 255.00 μm.

Instruments, Abingdon, Oxfordshire, UK) for energy dispersive microanalysis. The SEM stage was then calibrated for the Zeiss AxioVision 4.8 by finding the reference marks, setting the microscope for 3,000× magnification, and using the Everhart-Thornley (SE) electron detector at 8.5 mm of working distance. Finally, the image files corresponding to the picture with the larger focused area for each bright-field stack were loaded under the Zeiss AxioVision program, driving the SEM stage to almost the same (x, y) fields pictured with the light microscope. Images were then ac-

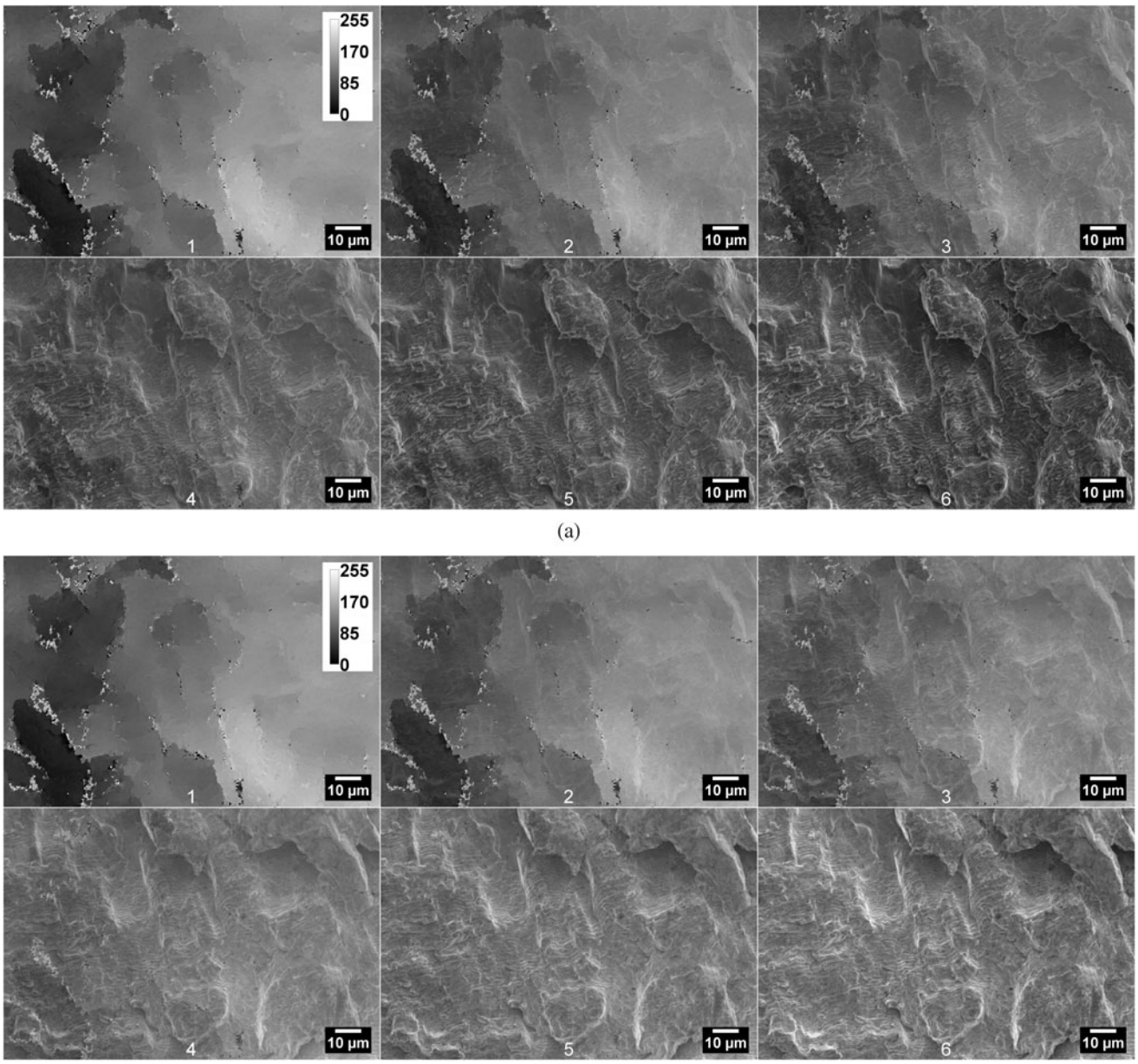

Figure 2. Example of the field matching precision: (**a**) morphing sequence from LM height map to 14 keV SEM-SE image produced by the iMorph plugin; (**b**) morphing sequence from LM height map to 2 keV SEM-SE image.

quired for SEs (at 2 keV and at 14 keV) and energy dispersive spectrometer (EDS) mapping also at a fixed working distance of 8.5 mm. These images were aligned with the light microscope using the Shuttle & Find plugin for Zeiss AxioVision 4.8.

The extended depth from focus reconstructions of LM image stacks was processed by the Michael Umorim's Stack Focuser plugin (http://imagej.nih.gov/ij/plugins/stack-focuser.html) for public domain NIH ImageJ 1.46p (Rasband, 2012) image processing and analysis program. This procedure description can be found in Caltabiano et al. (2012). Other tools for NIH ImageJ were also useful plugins for the analysis of images matching: the Hajime Hirase's "iMorph" (http://rsbweb.nih.gov/ij/plugins/morph.html) and the Interactive 3D Surface Plot (http://rsbweb.nih.gov/ij/plugins/surface-plot-3d.html) by Kai Uwe Barthel.

Results and Discussion

The main advantage of this technique is to combine the quantitative topographic information from the LM height maps to the fractographic features at SEM images, favored by the finest lateral resolution. Also, the aspects of fracture mechanisms can be compared between SEM and reconstructed LM images. The matching between LM and SEM regions was improved when the alignment of reference marks was executed under high magnification in the light microscope (1,600× in this work) and choosing the manual

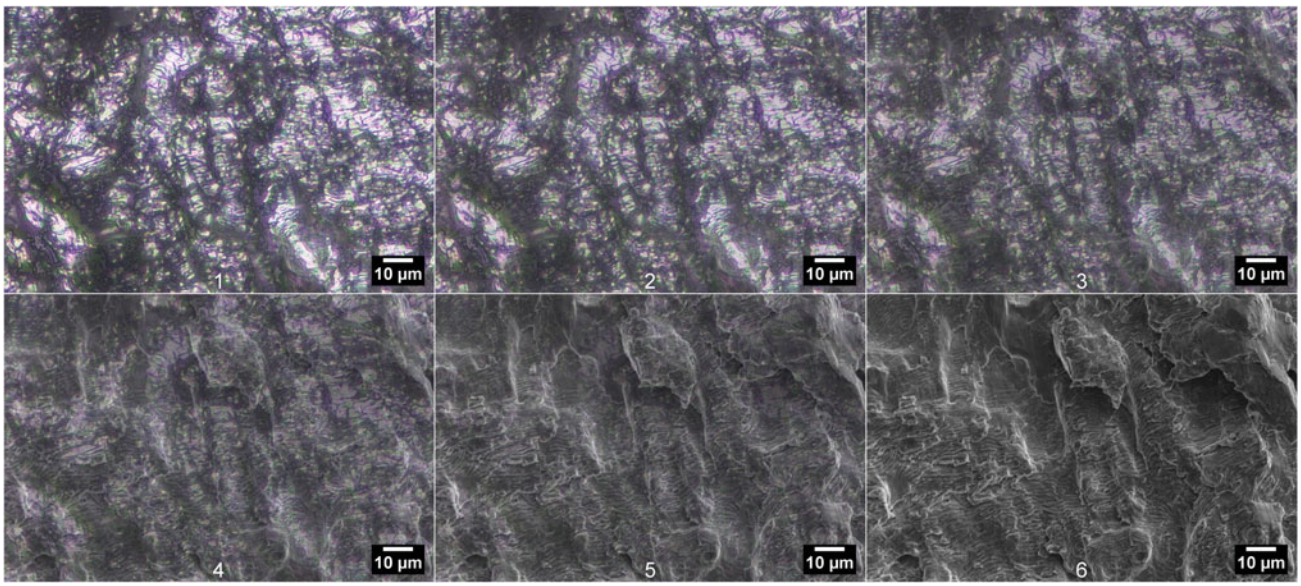

Figure 3. Morphing sequence from reconstructed LM image to 14 keV SEM-SE image produced by the iMorph plugin. This morphing tool provides an image sequence for the transformation of LM image to the SEM.

positioning option in the Shuttle & Find. The same care is recommended for the calibration of the SEM stage.

Figure 1 presents an example of the matching among a bright-field LM elevation map (Fig. 1a), the reconstructed LM image (Fig. 1b), and the corresponding SE image (Fig. 1c). Noise in elevation map reconstruction occurs mainly at vertical fracture steps, being coincident with edges in the SEM image (Fig. 1d). The noise filtered three-dimensional (3D) image (using smoothing slider of Interactive 3D Surface Plot plugin) in Figure 1e permits the analysis of the correlation between the topography formation and fracture micromechanisms. In this example, the fracture region is representative of fatigue crack propagation. It is formed mainly by transgranular fatigue striations, but with some few intergranular facets. It is evident that grain size influenced the local surface roughness. The intergranular facet formation is also favored by the solutes present at grain boundaries, as observed in the 3D image (Fig. 1f) of the correlation between the LM height map and the EDS map of chemical element distribution.

The SEs contrast can be better compared to the height map in Figure 2. Figure 2a is a morphing sequence from the LM height map to the 14 keV SEM-SE image produced by the iMorph plugin. The perfect matching is evidenced by the linear morphing technique, also demonstrating the influence of the collection of backscattered electrons (BSE) by the Everhart-Thornley detector (Chapman, 1999) and the edges shadowing on the apparent "topographic" contrast in the SEM image. The sequence in Figure 2b is for the morphing sequence from LM height map to 2 keV SEM-SE image. The edges shadowing is less pronounced in this case, and both SE and BSE signals emerge from a thin surface region, but the contrast is reduced and the topographic aspect is not so pronounced as at high voltages (Joy & Joy, 1996). These distortions in surface contrast on SEM images cannot be avoided by other techniques, such as the stereo-pair reconstruction (Hein, 2001; Kang et al., 2012).

In Figure 3, the morphing sequence involved the reconstructed LM image and the 14 keV SEM-SE image. Differences in fractographic interpretation are made clear with correlative fractography technique. The topography described by the SEM image is favored by the finest lateral resolution, but the changes in surface behavior are influenced by the contrast effects of collected signal. The LM reconstructed image is affected by light saturation and higher lateral resolution, but the representation of topography behavior is more realistic. There are some regions in the LM reconstructed image where the micromechanisms cannot be recognized such as at the intergranular facets. The comparison to the similar SEM image permits contouring of this restriction.

Conclusions

The correlative fractography technique provides conditions for the analyst to get the complete scenario for fracture analysis. This technique directly associates the quantitative and qualitative aspects of fractographic investigation and combines the benefits of SEM and LM. Many surface and material properties can be evaluated at the same context, regarding the range of information provided by the techniques associated with both LM and SEM. Finally, the correlative fractography can provide the general comprehension of the mechanisms involved in fracture processes, with the benefits of the association of different resolution scales and surface properties.

Acknowledgments

The financial support for this work was provided by the following Brazilian agencies: FAPESP (São Paulo Research

Foundation) and CNPq (National Council for Scientific and Technological Development).

References

Agronskaia, A.V., Valentijn, J.A., Driel, L.F., Schneijdenberg, C.T.W.M., Humbel, B.M., Henegouwen, P.M.P.B., Verkleij, A.J., Koster, A.J. & Gerritsen, H.C. (2008). Integrated fluorescence and transmission electron microscopy. *J Struct Biol* **164**, 183–189.

Caltabiano, P.C.R.O., Rosa, P.H.S., Campos, K.A. & Hein, L.R.O. (2012). Extended depth from focus reconstruction method for stretch zone measurement in 15-5PH steel. *Microsc Res Tech* **75**, 1155–1158.

Chapman, S.K. (1999). Optimising the performance of a tungsten hairpin scanning electron microscope. *Scanning Microscopy* **13**, 141–146.

Hein, L.R.O. (2001). Quantitative fractography by digital image processing: NIH Image macro tools for stereo pair analysis and 3-D reconstruction. *J Microsc* **204**, 17–28.

Joy, D.C. & Joy, C.S. (1996). Low voltage scanning electron microscopy. *Micron* **27**, 247–263.

Kang, K.W., Pereda, M.D., Canafoglia, M.E., Bilmes, P., Llorente, C. & Bonetto, R.D. (2012). Uncertainty studies of topographical measurements on steel surface corrosion by 3D scanning electron microscopy. *Micron* **43**, 387–395.

Plitzko, J.M., Rigort, A. & Leis, A. (2009). Correlative cryo-light microscopy and cryo-electron tomography: From cellular territories to molecular landscapes. *Current Opin Biotechnol* **20**, 83–89.

Rasband, W.S. (2012). ImageJ. Bethesda, MD: U.S. National Institutes of Health. Available at http://imagej.nih.gov/ij.

Sartori, A., Gatz, R., Beck, F., Rigort, A., Baumeister, W. & Plitzko, J.M. (2007). Correlative microscopy: Bridging the gap between fluorescence light microscopy and cryo-electron tomography. *J Struct Biol* **160**, 135–145.

Verkade, P. (2008). Moving EM: The Rapid Transfer System as a new tool for correlative light and electron microscopy and high throughput for high-pressure freezing. *J Microsc* **230**, 317–328.

Vicidomini, G., Gagliani, M.C., Cortese, K., Krieger, J., Buescher, P., Bianchini, P., Boccacci, P., Tacchetti, C. & Diaspro, A. (2010). A novel approach for correlative light electron microscopy analysis. *Microsc Res Techniq* **73**, 215–224.